SCIENTIFIC REPORTS

OPEN

A fast and accurate computational method for the linear-combination-based isotropic periodic sum

Received: 21 February 2018
Accepted: 16 July 2018
Published online: 08 August 2018

Kazuaki Z. Takahashi[1], Takuma Nozawa[2] & Kenji Yasuoka[2]

An isotropic periodic sum (IPS) is a powerful technique to reasonably calculate intermolecular interactions for wide range of molecular systems under periodic boundary conditions. A linear-combination-based IPS (LIPS) has been developed to attain computational accuracy close to an exact lattice sum, such as the Ewald sum. The algorithm of the original LIPS method has a high computational cost because it needs long-range interaction calculations in real space. This becomes a performance bottleneck for long-time molecular simulations. In this work, the combination of an LIPS and fast Fourier transform (FFT) was developed, and evaluated on homogeneous and heterogeneous molecular systems. This combinational approach of LIPS/FFT attained computational efficiency close to that of a smooth particle mesh Ewald while maintaining the same high accuracy as the original LIPS. We concluded that LIPS/FFT has great potential to extend the capability of IPS techniques for the fast and accurate computation of many types of molecular systems.

Molecular dynamics (MD) simulations continue to evolve. Recent advances in computer power and algorithmic developments have made it possible to simulate a wide range of molecular systems with reasonable time and length scales for scientific and industrial applications[1–5].

The computational accuracy of MD has been supported by established molecular models and intermolecular interaction calculation methods[6–14]. Importantly, the accuracy of long-range interaction calculations strongly affects to the accuracy of MD. Under the periodic boundary conditions (PBCs), long-range interactions are ordinally calculated using truncation or lattice sum methods. The simplicity and calculation efficiency are merits of truncation methods, but truncation of long-range interactions can be serious defects on simulating Lennard-Jones (LJ) liquids[15–17], aqueous[18–28], and macromolecular systems[29–43]. The reaction field method[44,45], the Wolf method and its modifications[46,47], and the smoothing and/or shifting cutoff methods are kinds of truncation methods that have serious defects for various systems (see above citations). The Ewald sum[48] is used as the most accurate lattice sum method. It incorporates PBCs using the discrete Fourier transform (DFT), but the reciprocal term is computationally expensive. The particle mesh Ewald (PME) and its modifications[49,50] are particle-particle/particle-mesh approaches that use fast Fourier transforms (FFT) for the Ewald sum, and the smooth PME (SPME)[50] is now the *de facto* standard lattice sum method. The SPME perform well for intermediate-sized systems ($N \sim 10^3 - 10^5$, where N is the number of particles)[51]. However, the SPME does not have a high performance for large systems ($N \sim 10^6$ or larger), because it is difficult for FFT to attain strong scaling on massively parallel machines[52,53]. The Barnes-Hut tree-code[54] and the fast multipole method[55] are lattice sum methods that use hierarchical tree structures. These tree-based method can attain stronger scaling than FFT because it does not contain reciprocal space calculations that require all-to-all communications on massively parallel machines[53]. The tree-based method has been applied for long-range interaction calculations of molecular simulations[52,56–70]. The Gaussian split Ewald sum[71] is a combination between the Ewald sum and Poisson equation solver, and can avoid all-to-all communications on massively parallel machines. Importantly, all the lattice sum methods are potentially subject to the symmetry effect that comes from the lattice-like repetition of the unit cell for PBC. This effect is especially troublesome when simulating macromolecular systems, where conformational distributions are sensitive to image interactions[38,40,72–80]. More research into the lattice sum method is required, and the symmetry effect should be carefully considered.

[1]Research Center for Computational Design of Advanced Functional Materials, National Institute of Advanced Industrial Science and Technology (AIST), Central 2, 1-1-1 Umezono, Tsukuba, Ibaraki, 305-8568, Japan. [2]Department of Mechanical Engineering, Keio University, 3-14-1 Hiyoshi, Kohoku-ku, Yokohama, Kanagawa, 223-8522, Japan. Correspondence and requests for materials should be addressed to K.Z.T. (email: kazu.takahashi@aist.go.jp)

To avoid the symmetry effect, the isotropic periodic sum (IPS) technique is a promising approach. It was first developed by Wu and Brooks[81]. The IPS has become a powerful technique to reasonably calculate intermolecular interactions for a wide range of molecular systems, including net-charge systems under PBCs. It has been applied to solids[82], liquids[81,83–86], solid–liquid[87,88] and liquid-vapor interfaces[89,90], liquid crystals[91], proteins[81,92], lipids[89,93], combined quantum mechanics/molecular mechanics methods[94], and constant pH MD simulations[95–97]. Improved methods have been developed for large-scale systems that exploit the possibility of parallel computing[98,99].

An extended IPS technique, that is, the linear-combination-based IPS (LIPS) was developed to improve the accuracy of the IPS for both homogeneous and heterogeneous systems[7,100–103]. The LIPS provides periodic reaction fields that can design pseudo pair potentials in the range of extended IPS theory. This pseudo pair potential has the high accuracy that achieves computational results close to an exact lattice sum. For example, in the phase transition of liquid crystal systems, the LIPS and SPME with fine grid spacing are the only techniques that can reasonably estimate the solid–liquid-crystalline phase transition temperature[104]. The LIPS has great potential as one of the best possible approaches to contribute to a further substantial advance in IPS techniques. However, the algorithm of the original LIPS has a high computational cost because it requires long-range interaction calculations in real space. This becomes a performance bottleneck for long-time molecular simulations using the LIPS. Several possible approaches to raise the computational efficiency of the LIPS were suggested in the original paper[100], but have not been applied.

In the present work, the combination of the LIPS and fast Fourier transform (FFT), that is, LIPS/FFT, is developed as a substantial advance in the computational efficiency of the LIPS for intermediate-sized systems ($N \sim 10^3 - 10^5$). The performance of LIPS/FFT is evaluated on homogeneous and heterogeneous polar molecular systems. LIPS/FFT attains computational efficiency close to the SPME while maintaining the high accuracy of the LIPS. We conclude that LIPS/FFT has great potential to extend the capability of IPS techniques for the fast and accurate computation of many types of molecular systems.

Methodology

LIPS/FFT method. In the LIPS method, pseudo pair potentials are designed using extended IPS theory, which provides periodic reaction fields[100,101]. Several types of pseudo pair potentials have been developed[100,101], and these can be expressed as the following equation generally:

$$u_{\mathrm{LIPS}}(r, R_c) = u(r) + \phi(r, R_c), \tag{1}$$

where u_{LIPS} is the LIPS pseudo pair potential; r is the interaction distance; R_c is the cutoff radius of the LIPS, which is closely related to the production of periodic reaction fields; u is an original pair potential, such as Coulomb interaction; and ϕ is the effective potential from the periodic reaction field. The LIPS pseudo pair potential has high accuracy. The previous paper demonstrated that one of the pseudo pair potentials, LIPS-SW, had the same accuracy as the SPME with fine grid spacing (less than 0.1 nm), for the estimation of the solid–liquid-crystalline phase transition temperature[104]. To attain high accuracy, the LIPS potentials require a large R_c condition $R_c = L/2$, where L is the length of the longest side of the simulation box. This means long-range interaction calculations in real space, and becomes a performance bottleneck for MD simulations using the LIPS. To avoid the aforementioned difficulty and attain advanced computational efficiency, the combination of the LIPS and FFT is developed as follows: (i) The original LIPS pair potential is divided into short-range, long-range and boundary pair potentials u_S, u_L and u_B, respectively. For the exact implementation within CHARMM[105–107] (version c40b2), the following expressions are used:

$$u_S(r, r_c) = \begin{cases} u_{\mathrm{LIPS}}(r, r_c) - u_{\mathrm{LIPS}}(r_c, r_c) & (r < r_c) \\ 0 & (r > r_c) \end{cases}, \tag{2}$$

$$u_L(r, r_c, R_c) = \begin{cases} u_{\mathrm{LIPS}}(r, R_c) - u_S(r, r_c) - u_B(r, R_c) & (r < R_c) \\ 0 & (r > R_c) \end{cases}, \tag{3}$$

$$u_B(r, R_c) = \begin{cases} u_{\mathrm{LIPS}}(R_c, R_c) & (r < R_c) \\ 0 & (r > R_c) \end{cases}. \tag{4}$$

where r_c ($<R_c$) is the short-range cutoff radius introduced for convenience. (ii) LIPS potential energy U_{LIPS} is calculated as the summation of the short-range, long-range, and boundary potential energy, U_S, U_L and U_B, respectively.

$$U_{\mathrm{LIPS}} = U_S + U_L + U_B. \tag{5}$$

(iii) The short-range potential energy U_S is simply calculated in real space:

$$U_S = \frac{1}{2}\sum_i^N q_i \sum_{r_{ij}<r_c} q_j u_S(r_{ij}, r_c), \tag{6}$$

where r_{ij} is the interaction distance between particles i and j. (iv) The long-range potential energy is calculated in reciprocal space using FFT. The details are very similar to those of the SPME[50]. For any simulation box, the charge distribution q and potential energy distribution Φ can be exactly defined using matrices that contain positional

information for point charges. For the advanced calculation efficiency of FFT, the point charges have to be redistributed to predefined grid points. To do this, the following charge array Q is introduced:

$$Q(k_1, k_2, k_3) = \sum_{i}^{N} \sum_{n_1,n_2,n_3} q_i M_n(w_{1i} - k_1 - n_1K_1) \times M_n(w_{2i} - k_2 - n_2K_2) \cdot M_n(w_{3i} - k_3 - n_3K_3), \tag{7}$$

where k_1, k_2, and k_3 are integers that correspond to predefined grid points; n_1, n_2, and n_3 are integers that correspond to the real space summation; M_n is the cardinal b-spline function of the n-th order; w_{1i}, w_{2i}, and w_{3i} are real numbers; and K_1, K_2, and K_3 are positive integers that correspond to the total number of grid points. Thus, the Fourier transform of q is approximated by Q as follows:

$$F(q)(m_1, m_2, m_3) \simeq b_1(m_2)b_1(m_2)b_3(m_3)F(Q)(m_1, m_2, m_3), \tag{8}$$

where F is the operator of the discrete Fourier transform (DFT); m_1, m_2, and m_3 are integers that correspond to the reciprocal space summation; and

$$b_i(m_i) = \frac{\exp(2\pi i(n-1)m_i/K_i)}{\sum_{k=0}^{n-2} M_n(k+1)\exp(2\pi i m_i k/K_i)}. \tag{9}$$

The term Φ for long-range pair potential at the grid points also has to be defined. Thus, the following energy array Φ^* is introduced:

$$\Phi^*(k_1, k_2, k_3) = \sum_{n_1,n_2,n_3} u_{\mathrm{L}}[r(k_1 + n_1K_1, k_2 + n_2K_2, k_3 + n_3K_3) - r(1, 1, 1), r_{\mathrm{c}}, R_{\mathrm{c}}]. \tag{10}$$

The convolution between Q and Φ^*, $Q * \Phi^*$, is expressed as follows:

$$Q * \Phi^*(j_1, j_2, j_3) = \sum_{k_1=0}^{K_1-1} \sum_{k_2=0}^{K_2-1} \sum_{k_3=0}^{K_3-1} Q(k_1, k_2, k_3) \cdot \Phi^*(j_1 - k_1, j_2 - k_2, j_3 - k_3), \tag{11}$$

where j_1, j_2, and j_3 are integers. With the fine grid spacing conditions, $Q * \Phi^*$ can be used as the approximation of $q\Phi$. For advanced computational efficiency, the convolution calculation using FFT is essential. $Q * \Phi^*$ can be simply calculated using DFT and inverse DFT (IDFT):

$$Q * \Phi^* = F^{-1}[F(Q * \Phi^*)] = K_1K_2K_3 \cdot F^{-1}[F(Q) \cdot F(\Phi^*)], \tag{12}$$

where F^{-1} is the operator of IDFT. Therefore, long-range potential energy U_{L} can be calculated as follows:

$$\begin{aligned} U_{\mathrm{L}} &= \frac{1}{2}\sum_i q_i \sum_j q_j u_{\mathrm{L}} = \frac{1}{2}\sum_i q_i q\Phi \\ &\simeq \frac{1}{2}\sum_i q_i \sum_{m_1=0}^{K_1-1}\sum_{m_2=0}^{K_2-1}\sum_{m_3=0}^{K_3-1} F^{-1}[b_1b_2b_3F(Q * \Phi^*)] \\ &= \frac{1}{2}\sum_i q_i K_1K_2K_3 \sum_{m_1=0}^{K_1-1}\sum_{m_2=0}^{K_2-1}\sum_{m_3=0}^{K_3-1} b_1b_2b_3F^{-1}[F(Q) \cdot F(\Phi^*)] \\ &\simeq \frac{1}{2}\sum_{m_1=0}^{K_1-1}\sum_{m_2=0}^{K_2-1}\sum_{m_3=0}^{K_3-1} BF^{-1}(Q)[F(Q) \cdot F(\Phi^*)], \end{aligned} \tag{13}$$

where $B = |b_1|^2 \cdot |b_2|^2 \cdot |b_3|^2$. The reciprocal long-range force is calculated using the differential of Eq. 13 with respect to position vector of charges r_i:

$$-\nabla_i U_{\mathrm{L}} = -\frac{\partial U_{\mathrm{L}}}{\partial r_{\alpha i}} \simeq -\sum_{m_1=0}^{K_1-1}\sum_{m_2=0}^{K_2-1}\sum_{m_3=0}^{K_3-1} \frac{\partial Q}{\partial r_{\alpha i}} F^{-1}[BF(Q) \cdot F(\Phi^*)], \tag{14}$$

where $r_{\alpha i}$ is the α ($=x, y, z$) component of the coordinate of molecule i, r_i. The term $\partial Q/\partial r_{\alpha i}$ can be calculated based on Eq. 7 from the property of the b-spline functions:

$$\frac{d}{dw}M_n(w) = M_{n-1}(w) - M_{n-1}(w-1), \tag{15}$$

where w is a real number. (v) The boundary potential energy U_{B} is simply calculated in real space:

$$U_{\mathrm{B}} = \frac{1}{2}\sum_i^N q_i \sum_{r_{ij}<R_{\mathrm{c}}} q_j u_{\mathrm{B}}(r_{ij}, R_{\mathrm{c}}). \tag{16}$$

The potential energy and force of LIPS/FFT is calculated from the aforementioned five steps. Note that a similar approach was performed by Wu and Brooks for the combination of the IPS and FFT (IPS/DFFT)[92].

Simulation conditions. To evaluate the capability of LIPS/FFT on homogeneous and heterogeneous polar molecular systems, MD simulations for bulk water and water-vapor interfacial systems were performed. For a careful evaluation of the effect of IPS techniques on long-range interaction calculations, all the following three simulation conditions were met. (i) LIPS/FFT was applied only for electrostatic interactions. LIPS-SW[101] and LIPS-5th[100] were used for the pseudo pair potential of LIPS/FFT. For comparison, IPS/DFFT and the SPME were also applied only for electrostatic interactions. The IPS method for non-polar systems (IPSn)[81] and polar systems (IPSp)[84] were used for IPS/DFFT. For all the aforementioned methods, the short-range cutoff radius for real space interaction calculations and the order for *b*-spline interpolations were set to 1.0 nm and 8, respectively. The factor α for the SPME[48–50] was set to 3.71692 nm^{-1}, which corresponds to the short-range cutoff radius. For the treatment of Lennard-Jones (LJ) interactions, the shifting/switching functions to the LJ forces were used[105–107], with the non-bonded cutoff and inner-cutoff equal to 1.0 nm and 0.99 nm, respectively. (ii) The large cutoff radii R_c less than or equal to $L/2$ were mainly used under cubic simulation boxes as a result of considering previous reports for the symmetry effect[79,80]. Even though IPS techniques are conceptually different from the lattice sum, LIPS/FFT and IPS/DFFT at infinite R_c is almost equal to the lattice sum. Moreover, these two methods at $R_c > L/2$ contain at least the nearest copy boxes of PBCs without any processing by IPS techniques. These facts imply the concern that the combination of IPS techniques and FFT cannot avoid the effect from PBCs when requiring large cutoff radii $R_c > L/2$ for accuracy. For a secure application, therefore, LIPS/FFT and IPS/DFFT should be used at $R_c \leq L/2$. (iii) Fine grid spacing less than or equal to 0.1 nm was used. as a result of considering the previous study for liquid-crystalline phase transition phenomena[104], which demonstrated that even using the SPME, fine grid spacing conditions (less than 0.1 nm) were required for the accurate estimation of the phase transition temperature of macromolecular systems. LIPS/FFT and IPS/DFFT under fine grid spacing conditions should be evaluated for future applications to complex macromolecular systems.

Bulk water systems were simulated with a constant molecular number, volume, and temperature condition[108–110]. The number of water molecules was 6,192, the size of the simulation box was 5.71 nm × 5.71 nm × 5.71 nm, and the temperature was 298.15 K. The extended simple point charge (SPC/E) model[111] was used for water molecules. The atoms in each water molecule were constrained by the SHAKE algorithm[112]. The Verlet leapfrog integrator[113] was used with a time step of 2 fs. All simulation systems were equilibrated prior to data acquisition, and the elapsed time after the equilibration was 1 ns.

The water-vapor interfacial systems were simulated with the constant molecular number, volume, and temperature condition. The number of water molecules was 13,500, the size of simulation box was 10.8 nm × 10.8 nm × 10.8 nm, and the temperature was 298.15 K. The SPC/E model was used for water molecules. The atoms in each water molecule were constrained by the SHAKE algorithm. The Verlet leapfrog integrator was used with a time step of 2 fs. All simulation systems were equilibrated prior to data acquisition, and the elapsed time after the equilibration was 15 ns.

All the aforementioned simulations were performed using CHARMM[105–107] (version c40b2) modified for LIPS/FFT implementation.

Results and Discussion

To directly evaluate the accuracy of the electrostatic forces calculated by LIPS/FFT, the following two steps were performed: (i) The instantaneous value of the electrostatic forces was calculated for each method using exactly the same coordinates of molecular systems that had been equilibrated using the SPME. Note that the coordinates were not equilibrated using any IPS techniques but using the SPME. (ii) The instantaneous value was compared with that of the SPME using the root-mean-squared deviation of the forces, δ_f, and the largest error of the forces, $e_{f,\max}$, defined as follows:

$$\delta_f^2 = \frac{\sum_i \sum_\alpha |f_{\alpha,i} - f_{\alpha,i,SPME}|^2}{3N - 1}, \tag{17}$$

$$e_{f,\max} = \max |f_{\alpha,i} - f_{\alpha,i,SPME}|, \tag{18}$$

where $f_{\alpha,i}$ and $f_{\alpha,i,\mathrm{SPME}}$ are instantaneous forces calculated by LIPS/FFT and the SPME, respectively. For the calculation of δ_f, grid spacing Δ for the SPME was set to 0.05 nm. δ_f and $e_{f,\max}$ for IPS/DFFT were also calculated for comparison. Figure 1(a) shows the R_c dependences of δ_f (top) and $e_{f,\max}$ (bottom) for bulk water systems for two grid spacing conditions: $\Delta = 0.1$ nm and 0.05 nm. Overall, the R_c dependences of δ_f and $e_{f,\max}$ were similar to each other method, with few exceptions. However, the results show that LIPS/FFT was in better agreement with the SPME than IPS/DFFT. With increasing R_c, δ_f and $e_{f,\max}$ decreased, except for the case using IPSn/DFFT with $\Delta = 0.1$ nm. This indicates that only IPSn/DFFT with $\Delta = 0.1$ nm barely improved its accuracy with increasing R_c. This very slow decay of δ_f and $e_{f,\max}$ was caused by the cutoff boundary condition of the IPSn pseudo pair potential. This boundary condition was too simple to accurately estimate polar molecular systems[100]. Using finer grid spacings can improved the accuracy of IPSn/DFFT to a level close to the other methods. With decreasing Δ, δ_f and $e_{f,\max}$ decreased, except for the case that used IPSp/DFFT. This indicates that only IPSp/DFFT could not improve its accuracy by choosing fine grid spacing less than 0.1 nm. The IPSp pseudo pair potential included a screening effect from the countercharge modeled on the typical structure of polar molecular systems. This screening effect smeared information for the charge distribution embedded in the fine grids, and then inhibited the accuracy improvement of IPSp/DFFT. Figure 1(b) shows the R_c dependences of δ_f (top) and $e_{f,\max}$ (bottom) for water-vapor interfacial systems for two grid spacing conditions: $\Delta = 0.1$ nm and 0.05 nm. It is obvious that LIPS/FFT was in much better agreement with the SPME than IPS/DFFT. δ_f and $e_{f,\max}$ started to drastically decrease when R_c exceeded the thickness of the water slab (~4 nm), with a few exceptions. This fast decay was because the

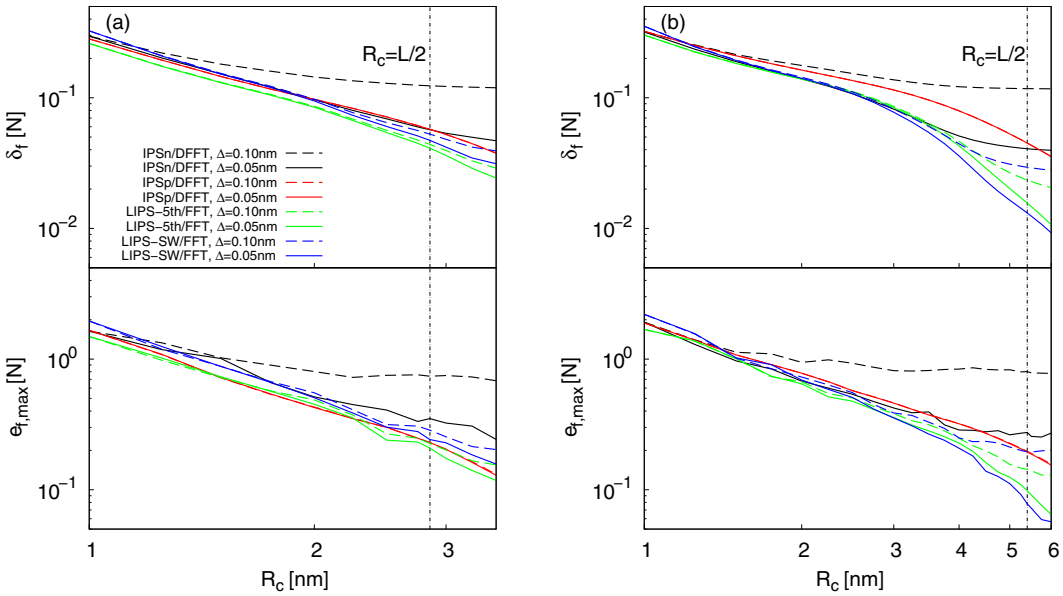

Figure 1. Cutoff radius R_c dependences of the root-mean-squared deviation of the forces δ_f (top) and the largest error of the forces $e_{f,max}$ (bottom) for (**a**) bulk water systems and (**b**) water-vapor interfacial systems. $R_c = L/2$ is also plotted.

sphere-like cutoff territory with large R_c became able to contain the major part of the characteristic structure of molecular systems. For LIPS/FFT, δ_f at $R_c > 4$ nm decayed in proportion to $R_c^{-3.4}$. For IPSp/DFFT, δ_f decay was clearly slower than it was for LIPS/FFT; δ_f at $R_c > 4$ nm decayed in proportion to $R_c^{-1.9}$. For IPSn/DFFT, δ_f decay was very slow. Using finer grid spacings could improve the accuracy of IPSn/DFFT; however, the slow decay tendency would still remain. Even using $\Delta = 0.05$ nm, δ_f at $R_c > 4$ nm barely decay. With decreasing Δ, δ_f and $e_{f,max}$ decreased, except for the case using IPSp/DFFT. Similar to the results of bulk water systems, only IPSp/DFFT could not improve its accuracy by choosing fine grid spacing less than 0.1 nm. The screening effect of IPSp inhibited accurate calculation using IPS/DFFT regardless of the homogeneity/heterogeneity of the molecular structure of systems.

To evaluate the accuracy of LIPS/FFT for estimating homogeneous/heterogeneous polar molecular systems, some physical properties for bulk water and water-vapor systems were calculated. The potential energy U is one of the fundamental thermodynamic properties. Figure 2(a) shows U for bulk water systems at $\Delta = 0.1$ nm. In comparison with the results of the SPME, the accuracy for estimating U is in the following order: LIPS-5th/FFT (=SPME) = LIPS-SW/FFT = IPSp/DFFT > IPSn/DFFT. This order follows the results of δ_f and $e_{f,max}$. The radial distribution function $g(r)$ is a critical property showing local configuration of molecular systems. The conventional expression give,

$$g(r) = \frac{V}{4\pi r^2 \Delta r N(N-1)} \sum_i n_i(r), \tag{19}$$

where $n_i(r)$ is the number of molecules in the region between r and $r + \Delta r$ from molecule i. Figure 2(b) shows the oxygen-oxygen $g(r)$ for bulk water systems at $R_c = 2.8$ nm and $\Delta = 0.1$ nm. In comparison with the results of the SPME, the accuracy for estimating $g(r)$ is in the following order: LIPS-5th/FFT (=SPME) = LIPS-SW/FFT = IPSp/DFFT > IPSn/DFFT. This order follows the results of δ_f and $e_{f,max}$. The velocity auto-correlation function $C(t)$ explains microscopic motion of molecular systems[114]. The conventional expression give,

$$C(t) = \frac{\sum_i v_i(t) \cdot v_i(0)}{\sum_i v_i(0) \cdot v_i(0)}, \tag{20}$$

where v_i is the velocity of molecule i. Figure 2(c) shows $C(t)$ for bulk water systems at $R_c = 2.8$ nm and $\Delta = 0.1$ nm. All the results were almost same as that of the SPME. The self-diffusion coefficient D is one of the representative dynamic properties. D can be determined either by the Einstein relation or Green-Kubo formula, which are basically equivalent. Here we used the Einstein relation,

$$D = \lim_{t\to\infty} \frac{1}{6Nt} \sum_i |r_i(t) - r_i(0)|^2, \tag{21}$$

where t is time. The slope of the mean-squared displacement of a diffusing particle in the long-time limit was calculated for the diffusion coefficient. Figure 2(d) shows D for bulk water systems at $\Delta = 0.1$ nm. All the results were almost same as that of the SPME. The mass density profile $\rho(z)$ is one of the fundamental thermodynamic properties showing the mass distribution of heterogeneous systems. Figure 2(e) shows $\rho(z)$ for water-vapor interfacial

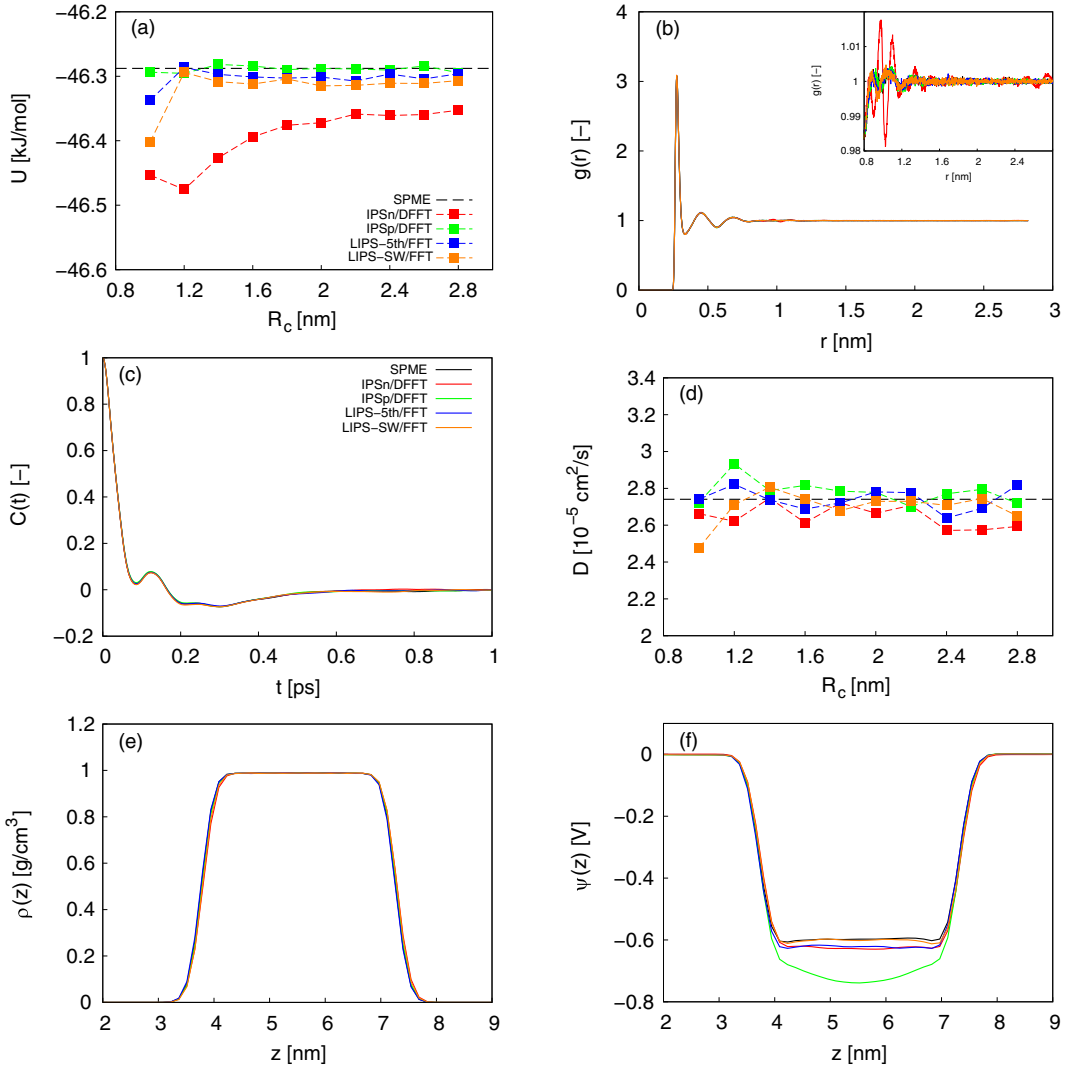

Figure 2. (**a**) Potential energy U for bulk water systems at $\Delta = 0.1$ nm. (**b**) Radial distribution function $g(r)$ for bulk water systems at $R_c = 2.8$ nm and $\Delta = 0.1$ nm. (**c**) Velocity auto-correlation function $C(t)$ for bulk water systems at $R_c = 2.8$ nm and $\Delta = 0.1$ nm. (**d**) Diffusion coefficient D for bulk water systems at $\Delta = 0.1$ nm. (**e**) Mass density profiles $\phi(z)$ for water-vapor interfacial systems at $R_c = L/2$ and $\Delta = 0.1$ nm. (**f**) Electrostatic potential profiles $\psi(z)$ for water-vapor interfacial systems at $R_c = L/2$ and $\Delta = 0.1$ nm.

systems at $R_c = L/2$ and $\Delta = 0.1$ nm. All the results were almost same as that of the SPME. The electrostatic potential profile $\psi(z)$ is well known as one of the properties sensitive to the cutoff radius[84,90,92,100–103], and thus should be calculated to evaluate the accuracy of the truncation methods. $\psi(z)$ was calculated using the double integration of the Poisson equation:

$$\psi(z) - \psi(0) = -\frac{1}{\varepsilon_0}\int_0^z \int_0^{z'} \rho_c(z'')dz''dz', \tag{22}$$

where z is the direction normal to the interface and ρ_c is the charge density profile for the z-direction. $\psi(0)$ on the left-hand side indicates a vacuum for liquid-vapor interfacial systems. Figure 2(f) shows $\psi(z)$ for water-vapor interfacial systems at $R_c = L/2$ and $\Delta = 0.1$ nm. The results of the electrostatic potential profile $\psi(z)$ for water-vapor interfacial systems do not always follow the results of δ_f and $e_{f,\max}$. In comparison with the results of the SPME, the accuracy for estimating $\psi(z)$ is in the following order: LIPS-SW/FFT (=SPME) > LIPS-5th/FFT = IPSn/DFFT > IPSp/DFFT. However, from Fig. 1(b), the accuracy for estimating δ_f and $e_{f,\max}$ at $R_c = L/2$ and $\Delta = 0.1$ nm is in the following order: LIPS-5th/FFT > LIPS-SW/FFT > IPSp/DFFT > IPSn/DFFT. There are two possible reasons for this difference. One is the influence of pseudo pair potentials at a relatively short interaction distance. For the pseudo pair potentials, the deviation from the Coulomb potential simply increased with an increase of the interaction distance. In a relatively short interaction distance ($r < R_c/2$), the deviation was in the following order: LIPS-SW < LIPS-5th = IPSn < IPSp. This fact corresponds to the results of $\psi(z)$, but not to that of δ_f and $e_{f,\max}$ because the deviation at a short interaction distance was concealed in δ_f and $e_{f,\max}$, which reflected

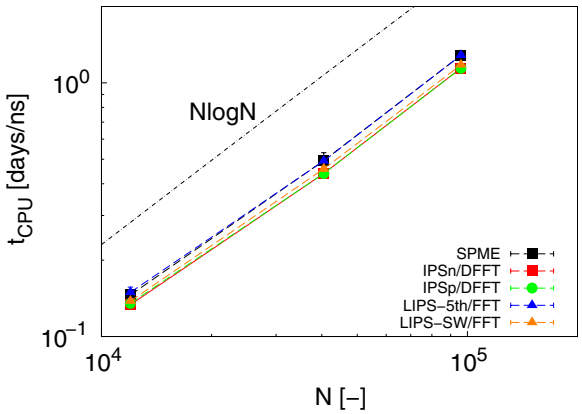

Figure 3. Number of charges N dependences on CPU time t_{CPU}. $O(N \log N)$ scaling is also plotted.

the total deviation. The other reason is the influence of the difference between the instantaneous and equilibrated values. δ_f and $e_{f,\max}$ are the instantaneous values calculated using coordinates equilibrated by the SPME, whereas $\psi(z)$ is the physical property calculated from the molecular structure equilibrated by each method. This difference may affect the evaluation of accuracy. Note that the results of $\psi(z)$ at $R_c = L/2$ and $\Delta = 0.05$ nm are almost the same as those plotted in Fig. 2(f), and consistent with the accuracy of δ_f and $e_{f,\max}$ at the same R_c and Δ conditions (data not shown).

To evaluate the computational efficiency of LIPS/FFT, CPU time t_{CPU} was measured for water-vapor interfacial systems with different N. An Intel(R) Xeon(R) CPU E5-2690 v2 (10 cores/20 threads, 3.00 GHz) was used for the measurement. L when $N = 12000$, 40500, and 96000 was 7.2 nm, 10.8 nm, and 14.4 nm, respectively. R_c and Δ were set to $L/2$ and 0.1 nm, respectively. Figure 3 shows the N dependence of t_{CPU}. The results clearly demonstrate that LIPS/FFT attained almost the same computational efficiency as the SPME. t_{CPU} for every method satisfied $O(N \log N)$ scaling, which means ideal computational efficiency using the FFT algorithm.

Conclusion

We developed a combination of the LIPS and FFT, LIPS/FFT, for a substantial advance in the computational efficiency of the LIPS for intermediate-sized systems ($N \sim 10^3 - 10^5$). The performance of LIPS/FFT was evaluated on homogeneous/heterogeneous polar molecular systems. LIPS/FFT attained computational efficiency almost the same as that of the SPME while maintaining the advanced accuracy of the original LIPS. Furthermore, static and dynamic properties calculated by LIPS-SW/FFT was almost the same as that by the SPME. This indicates that LIPS-SW/FFT accurately estimated not only instantaneous values but also equilibrated values. This high accuracy was observed within $R_c \leq L/2$. It clearly demonstrated that LIPS/FFT could overcome the concern that the combination of IPS techniques and FFT could not avoid the symmetry effect when requiring large cutoff radii $R_c > L/2$ for accuracy. One of the potential advantages of IPS techniques is the capability to simulate complex ionic systems that are difficult to accurately simulate using conventional lattice sum methods[79,80,115]. LIPS/FFT can enhance this advantage because it has both high accuracy and computational efficiency, while avoiding the symmetry effect. We conclude that the developed LIPS/FFT has great potential to extend the capability of IPS techniques for the fast and accurate computation of many types of molecular systems that involve highly complex ionic structure and dynamics, such as counterion condensation, ion conduction, and electrochemical migration. In further studies, the capability of LIPS/FFT for complex ionic systems will be intensively evaluated.

References

1. Perilla, J. R. *et al.* Molecular dynamics simulations of large macromolecular complexes. *Current opinion in structural biology* **31**, 64–74 (2015).
2. Dror, R. O., Dirks, R. M., Grossman, J., Xu, H. & Shaw, D. E. Biomolecular simulation: a computational microscope for molecular biology. *Annual review of biophysics* **41**, 429–452 (2012).
3. Dror, R. O. *et al.* Structural basis for nucleotide exchange in heterotrimeric g proteins. *Science* **348**, 1361–1365 (2015).
4. Chung, H. S., Piana-Agostinetti, S., Shaw, D. E. & Eaton, W. A. Structural origin of slow diffusion in protein folding. *Science* **349**, 1504–1510 (2015).
5. Lindorff-Larsen, K., Maragakis, P., Piana, S. & Shaw, D. E. Picosecond to millisecond structural dynamics in human ubiquitin. *The Journal of Physical Chemistry B* **120**, 8313–8320 (2016).
6. Schlick, T. *Molecular modeling and simulation: an interdisciplinary guide: an interdisciplinary guide*, vol. 21 (Springer Science & Business Media, 2010).
7. Cisneros, G. A., Karttunen, M., Ren, P. & Sagui, C. Classical electrostatics for biomolecular simulations. *Chemical Reviews* **114**, 779–814 (2014).
8. MacKerell Jr, A. D. *et al.* All-atom empirical potential for molecular modeling and dynamics studies of proteins. *The journal of physical chemistry B* **102**, 3586–3616 (1998).
9. Klauda, J. B. *et al.* Update of the charmm all-atom additive force field for lipids: validation on six lipid types. *The journal of physical chemistry B* **114**, 7830–7843 (2010).
10. Vanommeslaeghe, K. *et al.* Charmm general force field: A force field for drug-like molecules compatible with the charmm all-atom additive biological force fields. *Journal of computational chemistry* **31**, 671–690 (2010).
11. Cornell, W. D. *et al.* A second generation force field for the simulation of proteins, nucleic acids, and organic molecules. *Journal of the American Chemical Society* **117**, 5179–5197 (1995).

12. Lindorff-Larsen, K. *et al*. Improved side-chain torsion potentials for the amber ff99sb protein force field. *Proteins: Structure, Function, and Bioinformatics* **78**, 1950–1958 (2010).
13. Jorgensen, W. L., Madura, J. D. & Swenson, C. J. Optimized intermolecular potential functions for liquid hydrocarbons. *Journal of the American Chemical Society* **106**, 6638–6646 (1984).
14. Jorgensen, W. L., Maxwell, D. S. & Tirado-Rives, J. Development and testing of the opls all-atom force field on conformational energetics and properties of organic liquids. *Journal of the American Chemical Society* **118**, 11225–11236 (1996).
15. Smit, B. Phase diagrams of lennard-jones fluids. *The Journal of Chemical Physics* **96**, 8639–8640 (1992).
16. Trokhymchuk, A. & Alejandre, J. Computer simulations of liquid/vapor interface in lennard-jones fluids: Some questions and answers. *The Journal of chemical physics* **111**, 8510–8523 (1999).
17. Lopez-Lemus, J. & Alejandre, J. Thermodynamic and transport properties of simple fluids using lattice sums: bulk phases and liquid-vapour interface. *Molecular Physics* **100**, 2983–2992 (2002).
18. Neumann, M. & Steinhauser, O. The influence of boundary conditions used in machine simulations on the structure of polar systems. *Molecular Physics* **39**, 437–454 (1980).
19. Alper, H. E. & Levy, R. M. Computer simulations of the dielectric properties of water: Studies of the simple point charge and transferrable intermolecular potential models. *The Journal of Chemical Physics* **91**, 1242–1251 (1989).
20. Kitchen, D. *et al*. Conserving energy during molecular dynamics simulations of water, proteins, and proteins in water. *Journal of Computational Chemistry* **11**, 1169–1180 (1990).
21. Tasaki, K., McDonald, S. & Brady, J. Observations concerning the treatment of long-range interactions in molecular dynamics simulations. *Journal of computational chemistry* **14**, 278–284 (1993).
22. Smith, P. E. & van Gunsteren, W. F. Consistent dielectric properties of the simple point charge and extended simple point charge water models at 277 and 300 k. *The Journal of chemical physics* **100**, 3169–3174 (1994).
23. Feller, S., Pastor, R., Rojnuckarin, A., Bogusz, S. & Brooks, B. Effect of electrostatic force truncation on interfacial and transport properties of water. *The Journal of Physical Chemistry* **100**, 17011–17020 (1996).
24. van der Spoel, D., van Maaren, P. J. & Berendsen, H. J. A systematic study of water models for molecular simulation: derivation of water models optimized for use with a reaction field. *The Journal of chemical physics* **108**, 10220–10230 (1998).
25. Mark, P. & Nilsson, L. Structure and dynamics of liquid water with different long-range interaction truncation and temperature control methods in molecular dynamics simulations. *Journal of Computational Chemistry* **23**, 1211–1219 (2002).
26. Yonetani, Y. A severe artifact in simulation of liquid water using a long cut-off length: appearance of a strange layer structure. *Chemical Physics Letters* **406**, 49–53 (2005).
27. van der Spoel, D. & van Maaren, P. The origin of layer structure artifacts in simulations of liquid water. *Journal of Chemical Theory and Computation* **2**, 1–11 (2006).
28. Yonetani, Y. Liquid water simulation: A critical examination of cutoff length. *The Journal of Chemical Physics* **124**, 204501 (2006).
29. Loncharich, R. & Brooks, B. The effects of truncating long-range forces on protein dynamics. *Proteins: Structure, Function, and Bioinformatics* **6**, 32–45 (1989).
30. Schreiber, H. & Steinhauser, O. Cutoff size does strongly influence molecular dynamics results on solvated polypeptides. *Biochemistry* **31**, 5856–5860 (1992).
31. Schreiber, H. & Steinhauser, O. Molecular dynamics studies of solvated polypeptides: why the cut-off scheme does not work. *Chemical physics* **168**, 75–89 (1992).
32. Schreiber, H. & Steinhauser, O. Taming cut-off induced artifacts in molecular dynamics studies of solvated polypeptides* 1:: The reaction field method. *Journal of molecular biology* **228**, 909–923 (1992).
33. Saito, M. Molecular dynamics simulations of proteins in water without the truncation of long-range coulomb interactions. *Molecular Simulation* **8**, 321–333 (1992).
34. Guenot, J. & Kollman, P. Conformational and energetic effects of truncating nonbonded interactions in an aqueous protein dynamics simulation. *Journal of computational chemistry* **14**, 295–311 (1993).
35. Saito, M. Molecular dynamics simulations of proteins in solution: artifacts caused by the cutoff approximation. *The Journal of chemical physics* **101**, 4055–4061 (1994).
36. Oda, K., Miyagawa, H. & Kitamura, K. How does the electrostatic force cut-off generate non-uniform temperature distributions in proteins? *Molecular Simulation* **16**, 167–177 (1996).
37. Norberg, J. & Nilsson, L. On the truncation of long-range electrostatic interactions in dna. *Biophysical journal* **79**, 1537–1553 (2000).
38. Patra, M. *et al*. Molecular dynamics simulations of lipid bilayers: major artifacts due to truncating electrostatic interactions. *Biophysical Journal* **84**, 3636–3645 (2003).
39. Beck, D., Armen, R. & Daggett, V. Cutoff size need not strongly influence molecular dynamics results for solvated polypeptides. *Biochemistry* **44**, 609–616 (2005).
40. Monticelli, L., Simões, C., Belvisi, L. & Colombo, G. Assessing the influence of electrostatic schemes on molecular dynamics simulations of secondary structure forming peptides. *Journal of Physics: Condensed Matter* **18**, S329 (2006).
41. Reif, M., Kräutler, V., Kastenholz, M., Daura, X. & Hünenberger, P. Molecular dynamics simulations of a reversibly folding β-heptapeptide in methanol: influence of the treatment of long-range electrostatic interactions. *The Journal of Physical Chemistry B* **113**, 3112–3128 (2009).
42. Mazars, M. Long ranged interactions in computer simulations and for quasi-2d systems. *Physics Reports* **500**, 43–116 (2011).
43. Piana, S. *et al*. Evaluating the effects of cutoffs and treatment of long-range electrostatics in protein folding simulations. *PLoS One* **7**, e39918 (2012).
44. Barker, J. & Watts, R. Monte carlo studies of the dielectric properties of water-like models. *Molecular Physics* **26**, 789–792 (1973).
45. Watts, R. Monte carlo studies of liquid water. *Molecular Physics* **28**, 1069–1083 (1974).
46. Wolf, D., Keblinski, P., Phillpot, S. & Eggebrecht, J. Exact method for the simulation of coulombic systems by spherically truncated, pairwise 1/r summation. *The Journal of chemical physics* **110**, 8254–8282 (1999).
47. Fennell, C. J. & Gezelter, J. D. Is the ewald summation still necessary? pairwise alternatives to the accepted standard for long-range electrostatics. *The Journal of chemical physics* **124**, 234104 (2006).
48. Ewald, P. The calculation of optical and electrostatic grid potential. *Ann. Phys* **64**, 253–87 (1921).
49. Darden, T., York, D. & Pedersen, L. Particle mesh ewald: An N log (N) method for ewald sums in large systems. *The Journal of chemical physics* **98**, 10089–10092 (1993).
50. Essmann, U. *et al*. A smooth particle mesh ewald method. *The Journal of Chemical Physics* **103**, 8577–8593 (1995).
51. Frenkel, D. & Smit, B. *Understanding molecular simulation: from algorithms to applications*, vol. 1 (Academic Pr, 2002).
52. Kia, A., Kim, D. & Darve, E. Fast electrostatic force calculation on parallel computer clusters. *Journal of Computational Physics* **227**, 8551–8567 (2008).
53. Yokota, R., Barba, L. A., Narumi, T. & Yasuoka, K. Petascale turbulence simulation using a highly parallel fast multipole method on gpus. *Computer Physics Communications* **184**, 445–455 (2013).
54. Barnes, J. & Hut, P. A hierarchical 0 (n log n) force-calculation algorithm. *Nature* **324**, 4 (1986).
55. Greengard, L. & Rokhlin, V. A fast algorithm for particle simulations. *Journal of Computational Physics* **73**, 325–348 (1987).
56. Niedermeier, C. & Tavan, P. A structure adapted multipole method for electrostatic interactions in protein dynamics. *The Journal of chemical physics* **101**, 734 (1994).

57. Zhou, R. & Berne, B. A new molecular dynamics method combining the reference system propagator algorithm with a fast multipole method for simulating proteins and other complex systems. *The Journal of chemical physics* **103**, 9444 (1995).
58. Petersen, H. Accuracy and efficiency of the particle mesh ewald method. *The Journal of chemical physics* **103**, 3668 (1995).
59. Niedermeier, C. & Tavan, P. Fast version of the structure adapted multipole method–efficient calculation of electrostatic forces in protein dynamics. *Molecular simulation* **17**, 57–66 (1996).
60. Pollock, E. & Glosli, J. Comments on p 3 m, fmm, and the ewald method for large periodic coulombic systems. *Computer Physics Communications* **95**, 93–110 (1996).
61. Lambert, C. G., Darden, T. A. & Board, J. A. Jr A multipole-based algorithm for efficient calculation of forces and potentials in macroscopic periodic assemblies of particles. *Journal of Computational Physics* **126**, 274–285 (1996).
62. Lim, K. *et al*. Molecular dynamics for very large systems on massively parallel computers: the mpsim program. *Journal of Computational Chemistry* **18**, 501–521 (1997).
63. Eichinger, M., Grubm'ueller, H., Heller, H. & Tavan, P. Famusamm: An algorithm for rapid evaluation of electrostatic interactions in molecular dynamics simulations. *Journal of Computational Chemistry* **18**, 1729–1749 (1997).
64. Figueirido, F., Levy, R., Zhou, R. & Berne, B. Large scale simulation of macromolecules in solution: Combining the periodic fast multipole method with multiple time step integrators. *The Journal of Chemical Physics* **106**, 9835–9849 (1997).
65. Dimitrov, D. & Raev, N. Molecular dynamics simulations of the electrical double layer at the 1 m kcl solution | hg electrode interface. *Journal of Electroanalytical Chemistry* **486**, 1–8 (2000).
66. Wang, Z., Lupo, J., Patnaik, S. & Pachter, R. Large scale molecular dynamics simulations of a 4-n-pentyl-4′-cyanobiphenyl (5cb) liquid crystalline model in the bulk and as a droplet. *Computational and Theoretical Polymer Science* **11**, 375–387 (2001).
67. Mathias, G., Egwolf, B., Nonella, M. & Tavan, P. A fast multipole method combined with a reaction field for long-range electrostatics in molecular dynamics simulations: The effects of truncation on the properties of water. *The Journal of Chemical Physics* **118**, 10847 (2003).
68. Mathias, G. & Tavan, P. Angular resolution and range of dipole–dipole correlations in water. *The Journal of chemical physics* **120**, 4393 (2004).
69. Deng, S. & Cai, W. Extending the fast multipole method for charges inside a dielectric sphere in an ionic solvent: High-order image approximations for reaction fields. *Journal of computational physics* **227**, 1246–1266 (2007).
70. Lorenzen, K., Schwörer, M., Tröster, P., Mates, S. & Tavan, P. Optimizing the accuracy and efficiency of fast hierarchical multipole expansions for md simulations. *Journal of Chemical Theory and Computation* **8**, 3628–3636 (2012).
71. Shan, Y., Klepeis, J. L., Eastwood, M. P., Dror, R. O. & Shaw, D. E. Gaussian split ewald: A fast ewald mesh method for molecular simulation. *The Journal of chemical physics* **122**, 054101 (2005).
72. Roberts, J. & Schnitker, J. How the unit cell surface charge distribution affects the energetics of ion–solvent interactions in simulations. *The Journal of Chemical Physics* **101**, 5024–5031 (1994).
73. Roberts, J. & Schnitker, J. Boundary conditions in simulations of aqueous ionic solutions: a systematic study. *The Journal of Physical Chemistry* **99**, 1322–1331 (1995).
74. Luty, B. & Van Gunsteren, W. Calculating electrostatic interactions using the particle-particle particle-mesh method with nonperiodic long-range interactions. *The Journal of Physical Chemistry* **100**, 2581–2587 (1996).
75. Hünenberger, P. H. & McCammon, J. A. Ewald artifacts in computer simulations of ionic solvation and ion–ion interaction: a continuum electrostatics study. *The Journal of chemical physics* **110**, 1856–1872 (1999).
76. Hünenberger, P. & McCammon, J. Effect of artificial periodicity in simulations of biomolecules under ewald boundary conditions: a continuum electrostatics study. *Biophysical Chemistry* **78**, 69–88 (1999).
77. Weber, W., Hünenberger, P. & McCammon, J. Molecular dynamics simulations of a polyalanine octapeptide under ewald boundary conditions: influence of artificial periodicity on peptide conformation. *The Journal of Physical Chemistry B* **104**, 3668–3675 (2000).
78. Patra, M., Karttunen, M., Hyvönen, M., Falck, E. & Vattulainen, I. Lipid bilayers driven to a wrong lane in molecular dynamics simulations by subtle changes in long-range electrostatic interactions. *The Journal of Physical Chemistry B* **108**, 4485–4494 (2004).
79. Ye, X., Cai, Q., Yang, W. & Luo, R. Roles of boundary conditions in dna simulations: analysis of ion distributions with the finite-difference poisson-boltzmann method. *Biophysical journal* **97**, 554–562 (2009).
80. Lu, X. & Cui, Q. Charging free energy calculations using the generalized solvent boundary potential (gsbp) and periodic boundary condition: a comparative analysis using ion solvation and oxidation free energy in proteins. *The Journal of Physical Chemistry B* **117**, 2005–2018 (2013).
81. Wu, X. & Brooks, B. Isotropic periodic sum: A method for the calculation of long-range interactions. *The Journal of Chemical Physics* **122**, 044107 (2005).
82. Ojeda-May, P. & Pu, J. Assessing the accuracy of the isotropic periodic sum method through madelung energy computation. *The Journal of chemical physics* **140**, 164106 (2014).
83. Takahashi, K., Yasuoka, K. & Narumi, T. Cutoff radius effect of isotropic periodic sum method for transport coefficients of lennard-jones liquid. *The Journal of Chemical Physics* **127**, 114511 (2007).
84. Wu, X. & Brooks, B. Isotropic periodic sum of electrostatic interactions for polar systems. *The Journal of Chemical Physics* **131**, 024107 (2009).
85. Takahashi, K., Narumi, T. & Yasuoka, K. Cutoff radius effect of the isotropic periodic sum method in homogeneous system. ii. water. *The Journal of Chemical Physics* **133**, 014109 (2010).
86. Takahashi, K., Narumi, T. & Yasuoka, K. Cut-off radius effect of the isotropic periodic sum method for polar molecules in a bulk water system. *Molecular Simulation* **38**, 397–403 (2012).
87. Nakamura, H., Ohto, T. & Nagata, Y. Polarizable site charge model at liquid/solid interfaces for describing surface polarity: Application to structure and molecular dynamics of water/rutile tio2 (110) interface. *Journal of Chemical Theory and Computation* **9**, 1193–1201 (2013).
88. Ohto, T. *et al*. Influence of surface polarity on water dynamics at the water/rutile tio2 (110) interface. *Journal of physics. Condensed matter: an Institute of Physics journal* **26**, 244102–244102 (2014).
89. Klauda, J., Wu, X., Pastor, R. & Brooks, B. Long-range lennard-jones and electrostatic interactions in interfaces: application of the isotropic periodic sum method. *The Journal of Physical Chemistry B* **111**, 4393–4400 (2007).
90. Takahashi, K. Z., Narumi, T. & Yasuoka, K. Cutoff radius effect of the isotropic periodic sum and wolf method in liquid–vapor interfaces of water. *The Journal of Chemical Physics* **134**, 174112 (2011).
91. Nozawa, T., Takahashi, K. Z., Kameoka, S., Narumi, T. & Yasuoka, K. Application of isotropic periodic sum method for 4-pentyl-4′-cyanobiphenyl liquid crystal. *Molecular Simulation* **41**, 927–935 (2015).
92. Wu, X. & Brooks, B. Using the isotropic periodic sum method to calculate long-range interactions of heterogeneous systems. *The Journal of Chemical Physics* **129**, 154115 (2008).
93. Venable, R., Chen, L. & Pastor, R. Comparison of the extended isotropic periodic sum and particle mesh ewald methods for simulations of lipid bilayers and monolayers. *The Journal of Physical Chemistry B* **113**, 5855–5862 (2009).
94. Ojeda-May, P. & Pu, J. Isotropic periodic sum treatment of long-range electrostatic interactions in combined quantum mechanical and molecular mechanical calculations. *Journal of Chemical Theory and Computation* **10**, 134–145 (2014).
95. Wu, X. & Brooks, B. R. A virtual mixture approach to the study of multistate equilibrium: Application to constant ph simulation in explicit water. *PLoS Comput Biol* **11**, e1004480 (2015).

96. Wu, X., Lee, J. & Brooks, B. R. Origin of pka shifts of internal lysine residues in snase studied via equal-molar vmms simulations in explicit water. *The Journal of Physical Chemistry B* (2016).
97. Lee, J., Miller, B. T. & Brooks, B. R. Computational scheme for ph-dependent binding free energy calculation with explicit solvent. *Protein Science* **25**, 231–243 (2016).
98. Takahashi, K. Z., Narumi, T. & Yasuoka, K. A combination of the tree-code and ips method to simulate large scale systems by molecular dynamics. *Journal of Chemical Physics* **135**, 174108 (2011).
99. Wu, X., Pickard, F. C. IV & Brooks, B. R. Isotropic periodic sum for multipole interactions and a vector relation for calculation of the cartesian multipole tensor. *The Journal of Chemical Physics* **145**, 164110 (2016).
100. Takahashi, K. Z., Narumi, T., Suh, D. & Yasuoka, K. An improved isotropic periodic sum method using linear combinations of basis potentials. *Journal of Chemical Theory and Computation* **8**, 4503–4516 (2012).
101. Takahashi, K. Z. Design of a reaction field using a linear-combination-based isotropic periodic sum method. *Journal of computational chemistry* **35**, 865–875 (2014).
102. Takahashi, K. Z. & Yasuoka, K. A determination of liquid–vapour interfacial properties for methanol using a linear-combination-based isotropic periodic sum. *Molecular Simulation* **41**, 795–800 (2015).
103. Nozawa, T., Yasuoka, K. & Takahashi, K. Z. Critical test of isotropic periodic sum techniques with group-based cut-off schemes. *Scientific reports* **8**, 4185 (2018).
104. Nozawa, T., Takahashi, K. Z., Narumi, T. & Yasuoka, K. Comparison of the accuracy of periodic reaction field methods in molecular dynamics simulations of a model liquid crystal system. *Journal of computational chemistry* **36**, 2406–2411 (2015).
105. Brooks, B. R. *et al*. Charmm: a program for macromolecular energy, minimization, and dynamics calculations. *Journal of computational chemistry* **4**, 187–217 (1983).
106. MacKerell, A. D. *et al*. Charmm: the energy function and its parameterization. *Encyclopedia of computational chemistry* (1998).
107. Brooks, B. R. *et al*. Charmm: the biomolecular simulation program. *Journal of computational chemistry* **30**, 1545–1614 (2009).
108. Nosé, S. A molecular dynamics method for simulations in the canonical ensemble. *Molecular Physics* **52**, 255–268 (1984).
109. Nosé, S. A unified formulation of the constant temperature molecular dynamics methods. *The Journal of Chemical Physics* **81**, 511–519 (1984).
110. Hoover, W. G. Canonical dynamics: equilibrium phase-space distributions. *Physical Review A* **31**, 1695–1697 (1985).
111. Berendsen, H., Grigera, J. & Straatsma, T. The missing term in effective pair potentials. *Journal of Physical Chemistry* **91**, 6269–6271 (1987).
112. Ryckaert, J.-P., Ciccotti, G. & Berendsen, H. J. Numerical integration of the cartesian equations of motion of a system with constraints: molecular dynamics of n-alkanes. *Journal of Computational Physics* **23**, 327–341 (1977).
113. Hockney, R. W. The potential calculation and some applications. *Methods in Computational Physics* **9**, 135–211 (1970).
114. Balucani, U., Brodholt, J. & Vallauri, R. Analysis of the velocity autocorrelation function of water. *Journal of Physics: Condensed Matter* **8**, 6139 (1996).
115. Hub, J. S., de Groot, B. L., Grubm'uller, H. & Groenhof, G. Quantifying artifacts in ewald simulations of inhomogeneous systems with a net charge. *Journal of chemical theory and computation* **10**, 381–390 (2014).

Acknowledgements

We sincerely thank Dr. Ryuji Sakamaki of X-Ability Co., Ltd. for his great effort in implementing LIPS/FFT within CHARMM (version c40b2). KZT was supported in part by the Japan Society for the Promotion of Science (JSPS) Grants-in-Aid for Scientific Research (KAKENHI) Grant Number 16H06071. TN was supported in part by Grant-in-Aid for JSPS Fellows, and Ministry of Education, Culture, Sports, Science and Technology (MEXT) Grant-in-Aid for the Program for Leading Graduate Schools.

Author Contributions

K.Z.T. designed the project and developed the LIPS/FFT method; K.Z.T. and T.N. performed MD simulations and data analyses; K.Z.T. wrote the paper, and all authors contributed to the final version.

Additional Information

Competing Interests: The authors declare no competing interests.

Publisher's note: Springer Nature remains neutral with regard to jurisdictional claims in published maps and institutional affiliations.